

Non-Hermitian Weyl semimetals: Non-Hermitian skin effect and non-Bloch bulk-boundary correspondence

Xiaosen Yang(杨孝森), Yang Cao(曹阳), and Yunjia Zhai(翟云佳)
Citation: Chin. Phys. B, 2022, 31 (**1**): 010308. DOI: 10.1088/1674-1056/ac3738
Journal homepage: http://cpb.iphy.ac.cn; http://iopscience.iop.org/cpb

What follows is a list of articles you may be interested in

Exact solutions of non-Hermitian chains with asymmetric long-range hopping under specific boundary conditions

Cui-Xian Guo(郭翠仙) and Shu Chen(陈澍)
Chin. Phys. B, 2022, 31 (**1**): 010313. DOI: 10.1088/1674-1056/ac3228

Topology of a parity-time symmetric non-Hermitian rhombic lattice

Shumai Zhang(张舒迈), Liang Jin(金亮), and Zhi Song(宋智)
Chin. Phys. B, 2022, 31 (**1**): 010312. DOI: 10.1088/1674-1056/ac364a

Topological properties of non-Hermitian Creutz ladders

Hui-Qiang Liang(梁辉强) and Linhu Li(李林虎)
Chin. Phys. B, 2022, 31 (**1**): 010310. DOI: 10.1088/1674-1056/ac3991

Review of quantum simulation based on Rydberg many-body system

Zheng-Yuan Zhang(张正源), Dong-Sheng Ding(丁冬生), and Bao-Sen Shi(史保森)
Chin. Phys. B, 2021, 30 (**2**): 020307. DOI: 10.1088/1674-1056/abd744

A new way to construct topological invariants of non-Hermitian systems with the non-Hermitian skin effect

J S Liu(刘建森), Y Z Han(韩炎桢), C S Liu(刘承师)
Chin. Phys. B, 2020, 29 (**1**): 010302. DOI: 10.1088/1674-1056/ab5937

SPECIAL TOPIC — Non-Hermitian physics

Non-Hermitian Weyl semimetals: Non-Hermitian skin effect and non-Bloch bulk–boundary correspondence

Xiaosen Yang(杨孝森)[†], Yang Cao(曹阳), and Yunjia Zhai(翟云佳)

Department of physics, Jiangsu University, Zhenjiang 212013, *China*

(Received 23 August 2021; revised manuscript received 4 November 2021; accepted manuscript online 6 November 2021)

We investigate novel features of three-dimensional non-Hermitian Weyl semimetals, paying special attention to the unconventional bulk–boundary correspondence. We use the non-Bloch Chern numbers as the tool to obtain the topological phase diagram, which is also confirmed by the energy spectra from our numerical results. It is shown that, in sharp contrast to Hermitian systems, the conventional (Bloch) bulk–boundary correspondence breaks down in non-Hermitian topological semimetals, which is caused by the non-Hermitian skin effect. We establish the non-Bloch bulk–boundary correspondence for non-Hermitian Weyl semimetals: the topological edge modes are determined by the non-Bloch Chern number of the bulk bands. Moreover, these topological edge modes can manifest as the unidirectional edge motion, and their signatures are consistent with the non-Bloch bulk–boundary correspondence. Our work establishes the non-Bloch bulk–boundary correspondence for non-Hermitian topological semimetals.

Keywords: non-Hermitian skin effect, Weyl semimental, bulk–boundary correspondence

PACS: 03.65.Vf, 73.43.Nq, 73.20.At **DOI:** 10.1088/1674-1056/ac3738

1. Introduction

Topological phases are characterized by bulk topological invariant. Examples include topological insulators,[1–10] topological superconductors/superfluids,[11–18] and Weyl semimetal.[19–31] For equilibrium closed systems, described by Hermitian Hamiltonian, the topological invariants are defined in terms of the Bloch Hamiltonian.[3–5] The Hermitian Hamiltonian has real eigenenergies and a set of orthogonal eigenstates. The bulk topological invariants dictate the existence of robust edge states at the boundary. This bulk–boundary correspondence is a ubiquitous guiding principle to the topological phases. The bulk–boundary correspondence is also applicable when the bulk is gapless, by virtue of point touching of nondegenerate conduction and valence bands.[19] The gapless bulk band structure has paired Weyl points with opposite chirality and topological charge. The massless Weyl fermions near the Weyl points are stable against perturbations.

Recently, considerable efforts have been devoted to explore the properties of nonequilibrium open systems, especially non-Hermitian systems.[32–60] The non-Hermitian systems include optical and mechanical systems with gain and loss,[61–70] solid state systems with finite quasiparticle lifetimes for non-Hermitian self energy.[71–76] The non-Hermitian systems exhibit many impressive features, such as non-Hermitian skin effect,[77–87] bulk Fermi arcs connecting exceptional points[71,72,88,89] and biorthogonality.[90–93] Specifically, the non-Hermitian skin effect[77–82] means that all energy eigenstates can be localized at the boundary of non-Hermitian systems.[94–106] The interplay between the topology and non-Hermiticity can lead to the breakdown of the Bloch bulk–boundary correspondence.[77,78,81,82,105–109] The topological properties of the non-Hermitian systems can not be precisely predicted by the Bloch eigenstates under open boundary conditions. Furthermore, the real topological invariant is defined in non-Bloch Hamiltonian instead of Bloch Hamiltonian. The non-Bloch winding (Chern) number, defined in the generalized Brillouin zone (GBZ), has been introduced to characterize the topological properties of one-dimensional (two-dimensional) systems.[77,78,80,106] The non-Bloch topological invariants strictly characterize the chiral edge modes and provide the non-Bloch bulk–boundary correspondence.

For three-dimensional non-Hermitian systems, the Weyl points can be spread into exceptional lines and even exceptional surfaces. Examples of non-Hermitian Weyl semimetals have been considered in Refs. [40,48,110–117], however, their novel bulk–boundary correspondence has not been uncovered and clarified yet, which is the focus of the present paper. In this work, we investigate the topological properties of the non-Hermitian Weyl semimetal in the presence of gains and losses. We analyze the shape of the exceptional rings by Bloch band theory under periodic boundary condition and give the topological phase diagram. Furthermore, the Weyl semimetal can be regarded as a stack of layers of two-dimensional Chern insulator in k_z momentum space in the absence of gains and losses. Thus, we can bring insight into the topological properties of the non-Hermitian Weyl semimetal

[†]Corresponding author. E-mail: yangxs@ujs.edu.cn

© 2022 Chinese Physical Society and IOP Publishing Ltd

by the non-Bloch Chern number. We extend the Bloch momentum space $T^3(\boldsymbol{k})$ into complex momentum space $\tilde{T}^3(\tilde{\boldsymbol{k}})$ to derive the three-dimensional non-Bloch Hamiltonian. For a fixed momentum k_z, the three-dimensional complex momentum space $\tilde{T}^3(\tilde{\boldsymbol{k}})$ is reduced to two-dimensional $\tilde{T}^2(\tilde{\boldsymbol{k}}_\perp)$ in which the non-Bloch Chern number can be defined. We find a new non-Bloch bulk–boundary correspondence for the non-Hermitian Weyl semimetal. The non-Bloch Chern number can predict the topological edge modes. As such, the Bloch band theory and the conventional bulk–boundary correspondence break down for the non-Hermitian skin effect, which fundamentally affects the topological phase diagram. The validity of non-Bloch Chern number is confirmed by comparing its prediction to numerical results of real space energy spectra and edge-states transport.

2. Non-Hermitian Bloch Hamiltonian

We consider a non-Hermitian Bloch Hamiltonian of a semimetal on a cubic lattice

$$\begin{aligned} H(\boldsymbol{k}) = {} & (\sin k_x + \mathrm{i}\lambda)\sigma_x + (\sin k_y + \mathrm{i}\lambda)\sigma_y \\ & + (m - \cos k_x - \cos k_y - \cos k_z)\sigma_z, \end{aligned} \tag{1}$$

where $\sigma_{x,y,z}$ are the Pauli matrices. The real parameters $\boldsymbol{\Lambda} = (\lambda, \lambda, 0)$ are the non-Hermitian strengths.[77,118] In the absence of non-Hermitian parts ($\boldsymbol{\Lambda} = 0$), the eigenvalues of the system are $E_\pm(\boldsymbol{k}) = \pm h(\boldsymbol{k})$ with $h(\boldsymbol{k}) = |\boldsymbol{h}(\boldsymbol{k})|$ and $\boldsymbol{h}(\boldsymbol{k}) = (\sin k_x, \sin k_y, m - \cos k_x - \cos k_y - \cos k_z)$. A pair of Weyl points with Z_2 topological charge are stable when $|m| < 3$. The topological nontrivial phase is Weyl semimetal. When $|m| > 3$, the two Weyl points will annihilate with each other and the phase is gapped insulator. There is a topological phase transition between Weyl semimetal and insulator at $|m| = 3$. Therefore, we will focus on m being close to 3.

In the presence of the non-Hermitian parts, the Bloch energies of the above $H(\boldsymbol{k})$ are $E_\pm(\boldsymbol{k}) = \pm\sqrt{h(\boldsymbol{k})^2 - \boldsymbol{\Lambda}^2 + 2\mathrm{i}\boldsymbol{\Lambda}\cdot\boldsymbol{h}(\boldsymbol{k})}$. A non-Hermitian band is called fully gapped (or isolated) if the energy has no overlap with that of any other bands in the complex-energy plane, while it is called gapless (or inseparable) if the complex-energy is degenerate with other bands.[96] For our non-Hermitian system, the Bloch bands are gapless when $m < m_+$ with $m_\pm = 3 \pm \sqrt{2}\lambda$ as shown in Fig. 1. For the gapless regions, the phase is non-Hermitian Weyl semimetal and the Bloch spectra have a pair of Weyl exceptional rings with opposite charge[48,119] for periodic boundary condition when $m < m_-$. The two Weyl exceptional rings merge into one uncharged exceptional ring and the phase is topological trivial semimetal for $m_- < m < m_+$. There is a topological phase boundary between non-Hermitian Weyl semimetal and trivial semimetal at $m = m_-$. The uncharged exceptional ring will shrink into an exceptional point at $m = m_+$. Then, the phase is gapped insulator when $m > m_+$. Figure 2 shows the evolution of the exceptional rings with increasing m at $\lambda = 0.2$.

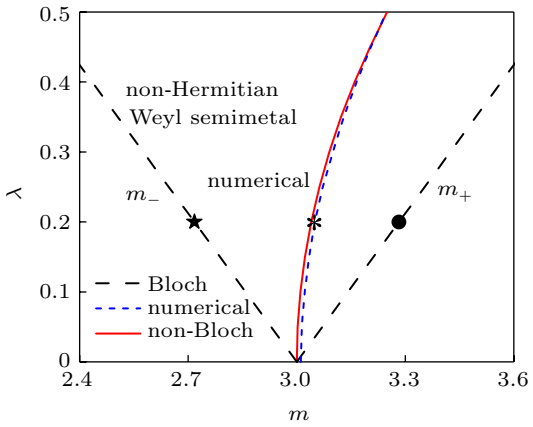


Fig. 1. Topological phase diagram for $\boldsymbol{\Lambda} = (\lambda, \lambda, 0)$. The blue-dotted curve, determined by the real space energy spectra of cubic open boundary, is the topological phase boundary between non-Hermitian Weyl semimetal and insulator. The left non-Hermitain Weyl semimetal has gapless bulk and gapless topological edge modes. The right insulator has gapped bulk and gapped edges. The open-boundary spectra for the three marked points are given in Fig. 3. The topological phase boundary closely approximates to the boundary based on non-Bloch Chern number (red-solid curve with $m = 3 + \lambda^2$). This non-Bloch phase boundary is fundamentally different from the phase boundaries based on the Bloch theory (black-dashed lines with $m_\pm = 3 \pm \sqrt{2}\lambda$). According to the Bloch band theory, the phase is non-Hermitian Weyl semimetal when $m < m_-$ and trivial semimetal for $m_- < m < m_+$. The phase is gapped insulator for $m > m_+$. The Bloch spectra have a pair of Weyl exceptional rings for non-Hermitian Weyl semimetal and a merged exceptional ring for trivial semimetal.

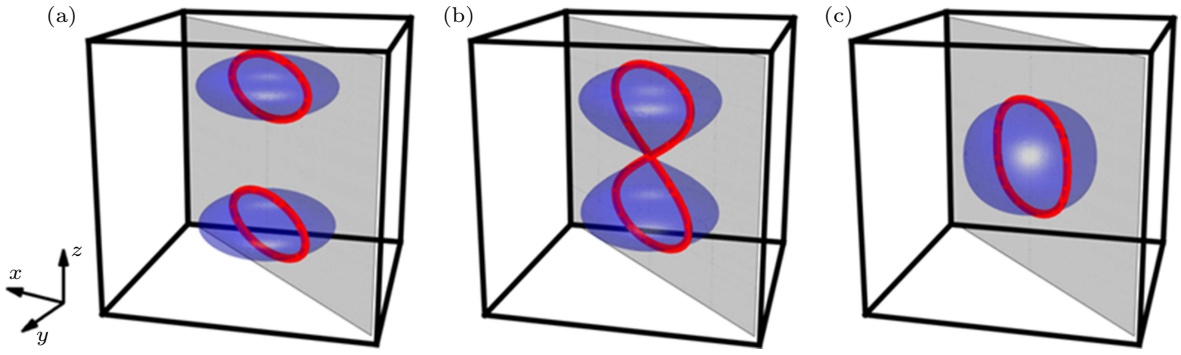


Fig. 2. Illustration of the exceptional rings in Bloch Brillouin zone with $\lambda = 0.2$ for (a) $m = 2.6$, (b) $m = 2.7172$, and (c) $m = 3.05$. In the presence of the non-Hermitian part, the paired Weyl points are spread into a pair of Weyl exceptional rings with opposite charge. As m increases, the two Weyl exceptional rings will merge into one uncharged exceptional ring at $m = m_-$. The uncharged exceptional ring will disappear when $m > m_+$.

3. Phase diagram based on non-Bloch Chern number

In Hermitian systems, Weyl semimetals are characterized by topologically protected Fermi-arcs. The chiral/helical gapless edge states exist in a finite region in momentum space and should be determined by the properties of Bloch Hamiltonian. The Bloch bulk–boundary correspondence is a key property of Weyl semimetals. However, the Bloch bulk–boundary correspondence is not applicable to the topological properties of the non-Hermitian system for non-Hermitian skin-effect. Therefore, the topological phase diagram based on the Bloch band theory will generate pronounced deviation to the real phase diagram. Thus, we draw the phase boundaries by the non-Bloch Chern number and the real space energy spectra.

The non-Bloch Chern number is defined in a complex momentum space instead of Bloch momentum space.[78] To determine the topological phase boundary, we consider the low-energy continuum case in x–y plane of our non-Hermitian Bloch Hamiltonian Eq.(1), which can be rewritten as following:

$$\begin{aligned} H(\boldsymbol{k}) &= (k_x + \mathrm{i}\lambda)\sigma_x + (k_y + \mathrm{i}\lambda)\sigma_y \\ &\quad + \left(m - 2 + \frac{k_x^2}{2} + \frac{k_y^2}{2} - \cos k_z\right)\sigma_z. \end{aligned} \tag{2}$$

The Bloch momentum space can be extended into complex momentum space by taking $k_{x,y} \to \tilde{k}_{x,y} + \mathrm{i}\tilde{k}'_{x,y}$ and $k_z \to \tilde{k}_z$. Here, the imaginary parts take the form $\tilde{k}'_{x,y} = -\lambda$.[78] The Bloch Brillouin zone $T^3(\boldsymbol{k})$ undergoes a deformation to GBZ $\tilde{T}^3(\tilde{\boldsymbol{k}})$. The non-Bloch Hamiltonian is defined as follows:

$$\begin{aligned} \tilde{H}(\tilde{\boldsymbol{k}}) &\equiv H(\boldsymbol{k} \to \tilde{\boldsymbol{k}} + \mathrm{i}\tilde{\boldsymbol{k}}') \\ &= \tilde{k}_x\sigma_x + \tilde{k}_y\sigma_y + \left[\tilde{m}(\tilde{k}_z) + \frac{\tilde{k}_x^2 + \tilde{k}_y^2}{2} - \mathrm{i}\lambda(\tilde{k}_x + \tilde{k}_y)\right]\sigma_z, \end{aligned}$$

with $\tilde{m}(\tilde{k}_z) = m - 2 - \lambda^2 - \cos\tilde{k}_z$. The right/left eigenvectors of the non-Hermitian Hamiltonian are $\left|u_{Rn}(\tilde{\boldsymbol{k}})\right\rangle / \left\langle u_{Ln}(\tilde{\boldsymbol{k}})\right|$ and satisfy

$$\begin{aligned} \tilde{H}(\tilde{\boldsymbol{k}})\left|u_{Rn}(\tilde{\boldsymbol{k}})\right\rangle &= E_n\left|u_{Rn}(\tilde{\boldsymbol{k}})\right\rangle, \\ \tilde{H}^{\dagger}(\tilde{\boldsymbol{k}})\left|u_{Ln}(\tilde{\boldsymbol{k}})\right\rangle &= E_n^*\left|u_{Ln}(\tilde{\boldsymbol{k}})\right\rangle, \end{aligned}$$

where n is the band index. The eigenvectors are normalized with $\langle u_{Ln}|u_{Rm}\rangle = \delta_{nm}$. We have $\tilde{k}_z = k_z$, which is real. For a fixed real value of k_z, the GBZ $\tilde{T}^3(\tilde{\boldsymbol{k}})$ is reduced to $\tilde{T}^2(\tilde{\boldsymbol{k}}_\perp)$ with $\tilde{\boldsymbol{k}}_\perp = (\tilde{k}_x, \tilde{k}_y)$. Then, we can use the definition of non-Bloch Chern number in two-dimensional GBZ $\tilde{T}^2(\tilde{\boldsymbol{k}}_\perp)$[78]

$$C_n(k_z) = \frac{1}{2\pi\mathrm{i}}\int_{\tilde{T}^2} \mathrm{d}^2\tilde{\boldsymbol{k}}_\perp \varepsilon^{i,j}\left\langle \partial_i u_{Ln}(\tilde{\boldsymbol{k}}_\perp, k_z)\middle|\partial_j u_{Rn}(\tilde{\boldsymbol{k}}_\perp, k_z)\right\rangle, \tag{3}$$

where $\varepsilon^{x,y} = -\varepsilon^{y,x} = 1$. For a fixed k_z, the non-Bloch bands are fully gapped. The non-Bloch Chern number is 0 for $\tilde{m}(k_z) > 0$ and 1 for $\tilde{m}(k_z) < 0$. When k_z changes, $C(k_z)$ remains constant as long as the gap is unclosed. $C(k_z)$ will change only when the gap is closed at $k_z = \pm k_z^c$ and the reduced plane $(\tilde{T}^2(\tilde{\boldsymbol{k}}_\perp))$ crosses non-Hermitian Weyl nodes. Like the case of Hermitian Weyl semimetal,[119] we can also assign an integer topological charge to each of the non-Hermitian Weyl nodes (equal to the change of the non-Bloch Chern number across the Weyl node). The topological charges stabilize the non-Hermitian Weyl nodes. Therefore, the topological phase boundary between non-Hermitian Weyl semimetal and insulator based on the non-Bloch Chern number is

$$m = 3 + \lambda^2, \tag{4}$$

which is shown in Fig. 1. The non-Hermitain Weyl semimetal phase on the left of the topological boundary has gapless bulk and gapless topological edge modes. The insulator phase on the right has gapped bulk and gapped edge modes. There is a dichotomy between the two topological phase diagrams based on the non-Bloch Chern number and the Bloch band theory. The exact topological phase boundary is only a single curve and the phase diagram has no topological trivial semimetal. Interesting, in sharp contrast to the Hermitian systems, the conventional bulk–boundary correspondence is broken down in the non-Hermitian Weyl semimetal phase. The topological edge modes of the non-Hermitian Weyl semimetal are determined by the non-Bloch Chern number of the bulk bands. The breakdown of the Bloch band theory is caused by the non-Hermitian skin effect.

To check the valid of the topological phase diagram based on non-Bloch Chern number, we calculate the real space energy spectra under cubic open-boundary condition (lattice sites size $L \times L \times L$). Figures 3(a)–3(c) show the spectra for (a) $m = 2.7172$, (b) $m = 3.05$, and (c) $m = 3.2828$ with $\lambda = 0.2$ (three indicated points in Fig. 1). Considering the size effects, we make the lattice size scaling of the gap in Figs. 3(d)–3(f) for Figs. 3(a)–3(c), respectively. The gap is given by the intercept of Δ–$1/L$ line. In Bloch theory, the three spectra are gapless and have exceptional rings/point in the spectra. As shown in Figs. 3(a) and 3(b), the gap vanishes for $m = 2.7172$ and $m = 3.05$ when $L \to \infty$. Remarkably, there is a clear gap at the spectra of $m = 3.2828$. According to the spectra of cubic open-boundary condition, there is a topological phase transition between the gapless non-Hermitian Weyl semimetal and gapped insulator phase at $m = 3.05$ for $\lambda = 0.2$. We draw the gapless-gaped phase boundary under cubic open-boundary condition as the blue-dotted curve in Fig. 1. The two curves base on the open-boundary energy spectra and the non-Bloch Chern number are very close. Therefore, the non-Bloch Chern number is valid to our three-dimensional non-Hermitian Weyl semimetal.

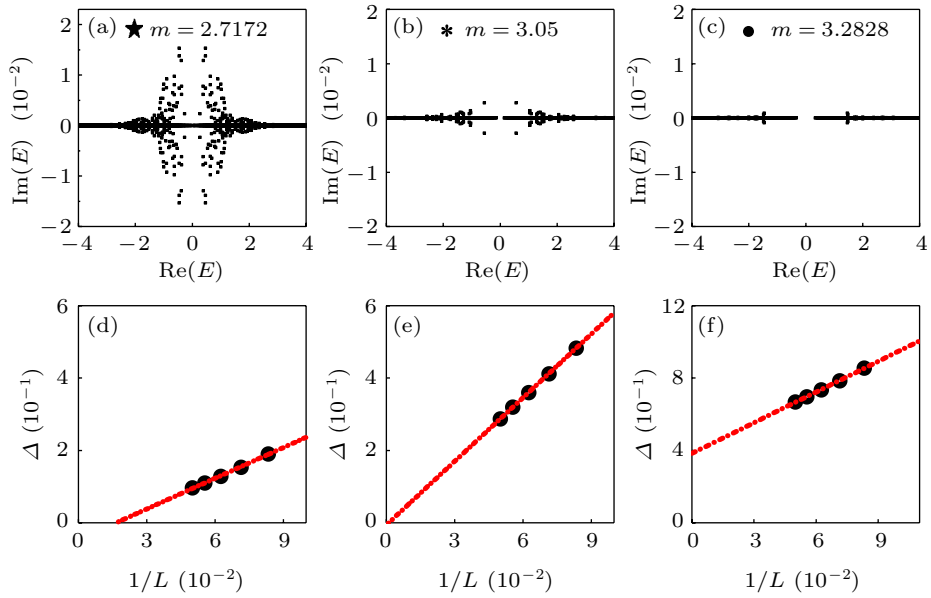


Fig. 3. Real space energy spectra under cubic open-boundary condition: (a) $m = 2.7172$, (b) $m = 3.05$, and (c) $m = 3.2828$ (three values of parameters indicated in Fig. 1) with $\lambda = 0.2$ and lattice site size $L = 20$. Panels (d)–(f) show the magnitude of the gap Δ as functions of $1/L$ for (a)–(c), respectively. L is the lattice site size in x, y, z direction. The intercept of Δ–$1/L$ line gives the gap in large scale limit ($L \to \infty$). The gap is zero for (d), (e) and nonzero for (f).

4. Non-Hermitian skin effect and unidirectional edge motion

Different from the Hermitian Hamiltonian, the eigenstates are non-orthogonal for the non-Hermitian cases. Therefore, all the eigenstates can be exponentially localized at the boundary for our non-Hermitian system. To illustrate the non-Hermitian skin effect, Fig. 4 shows the bulk states in x–y plane by adding up z-direction for (a) $m = 3.2828$ and (b) $m = 2.7172$ with $\lambda = 0.2$. The bulk states are localized at the boundary for both the non-Hermitian Weyl semimental and topological trivial gapped insulator phases. The usual bulk–boundary correspondence is invalid for our non-Hermitian systems.

For topological nontrivial phase, the localized eigenstates have Fermi-arc edge modes and gapless bulk states. However, there is no Fermi-arc edge mode in the topologically trivial regime. The chirality of the Fermi-arc edge modes will affect the wave pocket time evolution in topological nontrivial phases. To reveal the topological properties and the Fermi-arc edge modes, we investigate the wave pocket time evolution. The time dependent wave satisfies the non-Hermitian Schrödinger equation

$$\mathrm{i}\partial_t |\psi(t)\rangle = H |\psi(t)\rangle . \tag{5}$$

For an initial wave $|\psi(t=0)\rangle$, the time dependent wave function is $|\psi(t)\rangle = \sum_n \exp(-\mathrm{i}E_n t) |u_{Rn}\rangle \langle u_{Ln}|\psi(t=0)\rangle$.

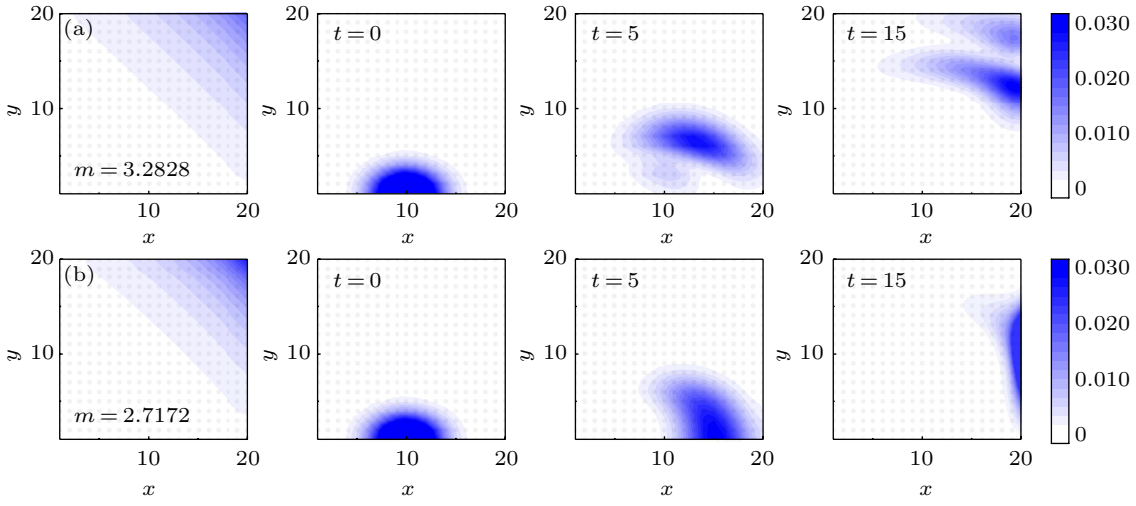


Fig. 4. Non-Hermitian skin effects. Left panel: total normalized eigenstates $\mathcal{N}_0 \sum_n |u_{Rn}\rangle$ under cubic open-boundary condition for (a) $m = 3.2828$ and (b) $m = 2.7172$ with $\lambda = 0.2$ and lattice sites size $L = 20$. Right panels: wave pocket evolutions. The initial wave pocket takes the Gaussian form $\psi(t=0) = \mathcal{N} \exp[-(i_x - 10)/20 - (i_y - 1)/10 - (i_z - 10)/20](1,1)^{\mathrm{T}}$, normalized by $\mathcal{N}$. The modulus squared intensity of $|\psi(t)\rangle$ is normalized and shown for $t = 0, 5, 15$ in x–y plane by adding up in z-direction. The wave packet fades into the bulk in up row. There has unidirectional edge motion in down row.

For simplicity, the initial wave takes Gaussian wave pocket with $\psi(t=0) = \mathcal{N}\exp[-(i_x-10)/20-(i_y-1)/10-(i_z-10)/20](1,1)^{\mathrm{T}}$, normalized by $\mathcal{N}$. As shown in Fig. 4, the wave pocket quickly spreads into the bulk for topological trivial insulator phase with $m = 3.2828$. However, there is clear chiral edge motion for the topological non-Hermitian Weyl semimetal with $m = 2.7172$. This can be explained as following. Despite the eigenstates are localized at the boundary for topological trivial phase, there is no robust chiral edge mode. Thus, the wave pocket evolves to the bulk states by quickly entering into the bulk without any topological constrain. For topological nontrivial phase, there are robust chiral edge modes with zero energy. The chirality of the edge modes will constrain the wave pocket evolution along the edges. The existence/absence of the unidirectional edge motion can be used to determine the non-Hermitian topological nontrivial phases in theory and future experiment.

5. Conclusion

We investigated the novel features of three-dimensional non-Hermitian Weyl semimetals by non-Bloch Chern number, Bloch band theory, open-boundary energy spectra and dynamics. We showed that the non-Hermitain Weyl semimetals have gapless bulk and gapless Fermi-arc edge modes. We uncovered the non-Bloch bulk–boundary correspondence for the non-Hermitian Weyl semimetal. The topological edge modes of the non-Hermitian Weyl semimetal are strictly determined by the non-Bloch Chern number of the bulk bands. Thus, the conventional bulk–boundary correspondence breaks down for the non-Hermitian skin effect. The non-Hermitian skin effect also generates pronounced deviation of the phase diagram from the Bloch band theory. The topological phase transition between nontrivial and trivial phases does not occur at the two Bloch phase boundaries. The topological phase boundary is only a single curve in the phase diagram. The valid of the non-Bloch Chern number is confirmed by the cubic open-boundary energy spectra. Furthermore, we showed that the topological edge modes can manifest as the unidirectional edge motion.

Acknowledgments

We would like to thank Zhong Wang for fruitful discussion. Project supported by the National Natural Science Foundation of China (Grants No. 11504143).

References

[1] Kane C L and Mele E J 2005 *Phys. Rev. Lett.* **95** 226801
[2] Bernevig B A, Hughes T L and Zhang S C 2006 *Science* **314** 1757
[3] Moore J E and Balents L 2007 *Phys. Rev. B* **75** 121306
[4] Fu L, Kane C L and Mele E J 2007 *Phys. Rev. Lett.* **98** 106803
[5] Qi X L, Hughes T L and Zhang S C 2008 *Phys. Rev. B* **78** 195424
[6] Hasan M Z and Kane C L 2010 *Rev. Mod. Phys.* **82** 3045
[7] Qi X L and Zhang S C 2011 *Rev. Mod. Phys.* **83** 1057
[8] Dzero M, Sun K, Galitski V and Coleman P 2010 *Phys. Rev. Lett.* **104** 106408
[9] Fu L 2011 *Phys. Rev. Lett.* **106** 106802
[10] Wang Z and Zhang S C 2012 *Phys. Rev. X* **2** 031008
[11] Qi X L, Hughes T L, Raghu S and Zhang S C 2009 *Phys. Rev. Lett.* **102** 187001
[12] Hor Y S, Williams A J, Checkelsky J G, Roushan P, Seo J, Xu Q, Zandbergen H W, Yazdani A, Ong N P and Cava R J 2010 *Phys. Rev. Lett.* **104** 057001
[13] Sasaki S, Kriener M, Segawa K, Yada K, Tanaka Y, Sato M and Ando Y 2011 *Phys. Rev. Lett.* **107** 217001
[14] Nakosai S, Tanaka Y and Nagaosa N 2012 *Phys. Rev. Lett.* **108** 147003
[15] Xu C and Balents L 2018 *Phys. Rev. Lett.* **121** 087001
[16] Zhang F, Kane C L and Mele E J 2013 *Phys. Rev. Lett.* **111** 056403
[17] Zhang W and Yi W 2013 *Nat. Commu.* **4** 2711
[18] Qu C, Zheng Z, Gong M, Xu Y, Mao L, Zou X, Guo G and Zhang C 2013 *Nat. Commun.* **4** 2710
[19] Wan X, Turner A M, Vishwanath A and Savrasov S Y 2011 *Phys. Rev. B* **83** 205101
[20] Burkov A A and Balents L 2011 *Phys. Rev. Lett.* **107** 127205
[21] Xu G, Weng H, Wang Z, Dai X and Fang Z 2011 *Phys. Rev. Lett.* **107** 186806
[22] Xu S Y, Belopolski I, Alidoust N, Neupane M, Bian G, Zhang C, Sankar R, Chang G, Yuan Z, Lee C C, Huang S M, Zheng H, Ma J, Sanchez D S, Wang B, Bansil A, Chou F, Shibayev P P, Lin H, Jia S, and Hasan M Z 2015 *Science* **349** 613
[23] Lv B Q, Weng H M, Fu B B, Wang X P, Miao H, Ma J, Richard P, Huang X C, Zhao L X, Chen G F, Fang Z, Dai X, Qian T and Ding H 2015 *Phys. Rev. X* **5** 031013
[24] Weng H, Fang C, Fang Z, Bernevig B A and Dai X 2015 *Phys. Rev. X* **5** 011029
[25] Young S M and Kane C L 2015 *Phys. Rev. Lett.* **115** 126803
[26] Sun X Q, Zhang S C and Wang Z 2015 *Phys. Rev. Lett.* **115** 076802
[27] Yan Z and Wang Z 2016 *Phys. Rev. Lett.* **117** 087402
[28] Bansil A, Lin H and Das T 2016 *Rev. Mod. Phys.* **88** 021004
[29] Armitage N P, Mele E J and Vishwanath A 2018 *Rev. Mod. Phys.* **90** 015001
[30] Chen Y, Xie Y, Gao Y, Chang P Y, Zhang S and Vanderbilt D 2018 *Phys. Rev. Materials* **2** 044205
[31] Gong C, Xie Y, Chen Y, Kim H S and Vanderbilt D 2018 *Phys. Rev. Lett.* **120** 106403
[32] Bender C M and Boettcher S 1998 *Phys. Rev. Lett.* **80** 5243
[33] Diehl S, Rico E, Baranov M A and Zoller P 2011 *Nat. Phys.* **7** 971
[34] Choi Y, Kang S, Lim S, Kim W, Kim J R, Lee J H and An K 2010 *Phys. Rev. Lett.* **104** 153601
[35] Malzard S, Poli C and Schomerus H 2015 *Phys. Rev. Lett.* **115** 200402
[36] Zhen B, Hsu C W, Igarashi Y, Lu L, Kaminer I, Pick A, Chua S L, Joannopoulos J D and Soljačić M 2015 *Nature* **525** 354
[37] Cao H and Wiersig J 2015 *Rev. Mod. Phys.* **87** 61
[38] Lee T E and Chan C K 2014 *Phys. Rev. X* **4** 041001
[39] Zhu B, Lü R, and Chen S 2014 *Phys. Rev. A* **89** 062102
[40] Xu Y, Wang S T and Duan L M 2017 *Phys. Rev. Lett.* **118** 045701
[41] Cai J Q, Xue Z Y, Gong M, Guo G C and Hu Y 2018 arXiv: 1812.02610
[42] Yoshida T, Peters R and Kawakami N 2018 *Phys. Rev. B* **98** 035141)
[43] Gong Z, Ashida Y, Kawabata K, Takasan K, Higashikawa S and Ueda M 2018 *Phys. Rev. X* **8** 031079
[44] Lee C H, Li G, Liu Y, Tai T, Thomale R and Zhang X 2018 arXiv:1812.02011
[45] Chen Y and Zhai H 2018 *Phys. Rev. B* **98** 245130
[46] Zhu W, Fang X, Li D, Sun Y, Li Y, Jing Y and Chen H 2018 *Phys. Rev. Lett.* **121** 124501
[47] Carlström J, Stålhammar M, Budich J C and Bergholtz E J 2019 *Phys. Rev. B* **99** 161115
[48] Cerjan A, Xiao M, Yuan L and Fan S 2018 *Phys. Rev. B* **97** 075128
[49] Parto M, Wittek S, Hodaei H, Harari G, Bandres M A, Ren J, Rechtsman M C, Segev M, Christodoulides D N and Khajavikhan M 2018 *Phys. Rev. Lett.* **120** 113901
[50] Yin C, Jiang H, Li L, Lü R and Chen S 2018 *Phys. Rev. A* **97** 052115
[51] Zhang S Y, Gong M, Guo G C and Zhou Z W 2020 *Phys. Rev. B* **101** 155150
[52] Liu T, Zhang Y R, Ai Q, Gong Z, Kawabata K, Ueda M and Nori F 2019 *Phys. Rev. Lett.* **122** 076801

[53] Kawabata K, Higashikawa S, Gong Z, Ashida Y and Ueda M 2019 *Nat. Commun.* **10** 297
[54] Yang Z and Hu J 2019 *Phys. Rev. B* **99** 081102
[55] Mu S, Lee C H, Li L and Gong J 2020 *Phys. Rev. B* **102** 081115
[56] Lee C H, Li L, Thomale R and Gong J 2020 *Phys. Rev. B* **102** 085151
[57] Mc Clarty P A and Rau J G 2019 *Phys. Rev. B* **100** 100405
[58] Ghatak A and Das T 2019 *J. Phys.: Condens. Matter* **31** 263001
[59] Liu J, Han Y and Liu C 2019 *Chin. Phys. B* **28** 100304
[60] Jiang X P, Qiao Y and Cao J 2021 *Chin. Phys. B* **30** 077101
[61] Makris K G, El-Ganainy R, Christodoulides D N and Musslimani Z H 2008 *Phys. Rev. Lett.* **100** 103904
[62] Klaiman S, U Günther and Moiseyev N 2008 *Phys. Rev. Lett.* **101** 080402
[63] Longhi S 2009 *Phys. Rev. Lett.* **103** 123601
[64] Rüter C E, Makris K, El-Ganainy G R, Christodoulides D N, Segev M and Kip D 2010 *Nat. Phys.* **6** 192
[65] Liertzer M, Ge L, Cerjan A, Stone A D, Türeci H E and Rotter S 2012 *Phys. Rev. Lett.* **108** 173901
[66] Regensburger A, Bersch C, Miri M A, Onishchukov G, Christodoulides D N and Peschel U 2012 *Nature* **488** 167
[67] Peng B, Özdemir S K, Rotter S, Yilmaz H, Liertzer M, Monifi F, Bender C M, Nori F and Yang L 2014 *Science* **346** 328
[68] Lu L, Joannopoulos J D and Soljačić M 2014 *Nat. Photon.* **8** 821
[69] Fleury R, Sounas D and Alù A 2015 *Nat. Commu.* **6** 5905
[70] Jiang X , Qiao Y and Cao J 2021 *Chin. Phys. B* **30** 077101
[71] Kozii V and Fu L 2017 arXiv:1708.05841
[72] Zhou H, Peng C, Yoon Y, Hsu C W, Nelson K A, Fu L, Joannopoulos J D, Soljačić M and Zhen B 2018 *Science* **359** 1009
[73] Zyuzin A A and Zyuzin A Y 2018 *Phys. Rev. B* **97** 041203
[74] Papaj M, Isobe H and Fu L 2019 *Rev. B* **99** 201107
[75] Zyuzin A A and Simon P 2019 *Phys. Rev. B* **99** 165145
[76] Moors K, Zyuzin A A, Zyuzin A Y, Tiwari R P and Schmidt T L 2019 *Phys. Rev. B* **99** 041116
[77] Yao S and Wang Z 2018 *Phys. Rev. Lett.* **121** 086803
[78] Yao S, Song F and Wang Z 2018 *Phys. Rev. Lett.* **121** 136802
[79] Song F, Yao S and Wang Z 2019 *Phys. Rev. Lett.* **123** 170401
[80] Song F, Yao S and Wang Z 2019 *Phys. Rev. Lett.* **123** 246801
[81] Lee C H and Thomale R 2019 *Phys. Rev. B* **99** 201103
[82] Martinez Alvarez V M, Barrios Vargas J E, Berdakin M and Foa Torres L E F 2018 *EPJ-Special Topics* **227** 1295
[83] Martinez Alvarez V M, Barrios Vargas J E and Foa Torres L E F 2018 *Phys. Rev. B* **97** 121401
[84] Xiao L, Deng T, Wang K, Zhu G, Wang Z, Yi W and Xue P 2020 *Nat. Phys.* **16** 761
[85] Helbig T, Hofmann T, Imhof S, Abdelghany M, Kiessling T, Molenkamp L W, Lee C H, Szameit A, Greiter M and Thomale R 2020 *Nat. Phys.* **16** 747
[86] Song F, Yao S and Wang Z 2019 *Phys. Rev. Lett.* **123** 170401
[87] Zhang K, Yang Z and Fang C 2020 *Phys. Rev. Lett.* **125** 126402
[88] Luo K, Feng J, Zhao Y X and Yu R 2018 arXiv: 181009231
[89] Carlström J and Bergholtz E J 2018 *Phys. Rev. A* **98** 042114
[90] Sokolov A V, Andrianov A A and Cannata F 2006 *J. Phys. A Math. Gen.* **39** 10207
[91] Kunst F K, Edvardsson E, Budich J C and Bergholtz E J 2018 *Phys. Rev. Lett.* **121** 026808
[92] Qiu X, Deng T S, Hu Y, Xue P and Yi W 2019 *iScience* **20** 392
[93] Edvardsson E, Kunst F K and Bergholtz E J 2019 *Phys. Rev. B* **99** 081302
[94] Lee T E 2016 *Phys. Rev. Lett.* **116** 133903
[95] Xiong Y 2018 *J. Phys. Commun.* **2** 035043
[96] Shen H and Fu L 2018 *Phys. Rev. Lett.* **121** 026403
[97] Wang B X and Zhao C Y 2018 *Phys. Rev. B* **98** 165435
[98] Wang H, Ruan J and Zhang H 2019 *Phys. Rev. B* **99** 075130
[99] Lee C H, Li L and Gong J 2019 *Phys. Rev. Lett.* **123** 016805
[100] Jiang H, Lang L J, Yang C, Zhu S L and Chen S 2019 *Phys. Rev. B* **100** 054301
[101] Ezawa M 2019 *Phys. Rev. B* **100** 045407
[102] Borgnia D S, Jura Kruchkov A and Slager R J 2020 *Phys. Rev. Lett.* **124** 056802
[103] Luo X W and Zhang C 2019 *Phys. Rev. Lett.* **123** 073601
[104] Deng T S and Yi W 2019 *Phys. Rev. B* **100** 035102
[105] Ghatak A and Das T 2019 *J. Phys.s: Condens. Matter* **31** 263001
[106] Yokomizo K and Murakami S 2019 *Phys. Rev. Lett.* **123** 066404
[107] Li L, Lee C H, Mu S and Gong J 2020 *Nat. Commun.* **11** 5491
[108] Jin L and Song Z 2019 *Phys. Rev. B* **99** 081103
[109] Kawabata K, Shiozaki K and Ueda M 2018 *Phys. Rev. B* **98** 165148
[110] Zyuzin A A and Zyuzin A Y 2018 *Phys. Rev. B* **97** 041203
[111] Carlström J and Bergholtz E J 2018 *Phys. Rev. A* **98** 042114
[112] Cerjan A, Huang S, Chen K P, Chong Y and Rechts-man M C 2019 *Nature Photonics* **13** 623
[113] Budich J C, Carlström J, Kunst F K, and Bergholtz E J 2019 *Phys. Rev. B* **99** 041406
[114] Carlström J, Stålhammar M, Budich J C and Bergholtz E J 2019 *Phys. Rev. B* **99** 161115
[115] Moors K, Zyuzin A A, Zyuzin A Y, Tiwari R P and Schmidt T L 2019 *Phys. Rev. B* **99** 041116
[116] Bergholtz E J and Budich J C 2019 *Phys. Rev. Research* **1** 012003
[117] Yoshida T, Peters R, Kawakami N and Hatsugai Y 2019 *Phys. Rev. B* **99** 121101
[118] Martinez Alvarez V M, Barrios Vargas J E and Foa Torres L E F 2018 *Phys. Rev. B* **97** 121401
[119] Morimoto T and Furusaki A 2014 *Phys. Rev. B* **89** 235127